JOURNAL OF GEOPHYSICAL RESEARCH, VOL. 98, NO. B2, PAGES 1759–1775, FEBRUARY 10, 1993

Beyond the Born and Rytov Approximations: A Nonlinear Approach to Electromagnetic Scattering

TAREK M. HABASHY, ROSS W. GROOM, AND BRIAN R. SPIES

Schlumberger-Doll Research, Ridgefield, Connecticut

The Born and Rytov approximations, widely used for solving scattering problems, are of limited utility for low-frequency electromagnetic scattering in geophysical applications where conductivity can vary over many orders of magnitude. We present four new, relatively simple nonlinear estimators that can be used for rapid electromagnetic modeling. The first, termed the static localized nonlinear approximation, is designed specifically to correct the magnitude of the electric field internal to the scatterer. The second, termed the localized nonlinear approximation, improves the estimate of the phase of the scattered field and includes some of the cross-polarization effects due to full wave scattering. Two further new estimators, based on the Rytov transformation (the localized nonlinear Rytov and the static localized nonlinear Rytov approximations) are designed to further improve the estimation of the phase of the scattered field, especially at high frequency and for larger size scatterers. Although these approximations are nonlinear functions in conductivity, they are generally much faster to compute than the full forward problem, and are almost as efficient as the Born or Rytov approximations. Moreover, the enhanced accuracy of the new estimators has made us optimistic about their application to low-frequency three-dimensional inverse problems in electromagnetics. The approximations developed in this paper will also be applicable to fields such as quantum mechanics, optics, ultrasonics, and seismology.

INTRODUCTION

The Born and Rytov approximations are widely used for solving scattering problems in acoustics, elastodynamics, electromagnetics and quantum mechanics. The Born approximation and the Born series were developed by M. Born in 1926 [*Born*, 1933] in connection with the solution of what is now known as the Lippmann-Schwinger integral equation that describes many-body scattering in quantum mechanics. The original Born approximation dealt with the scattering of a plane wave by a localized scatterer in a homogeneous medium (the background medium). Now, it has come to denote any approximation of the integral equation of scattering in which the total field in the integral over the scattering volume is approximated by the field in the background medium. When the background medium is more complex than a homogeneous medium (e.g., a layered medium), the approximation is usually called the distorted-wave Born approximation. In fact, for electromagnetic problems, an approximation using the background field as the internal electric field in the scattering integral was developed by Lord Rayleigh in 1881 [*Jackson*, 1975].

Approximating the total internal electric field by the background field is reasonable for small material contrasts as long as the scatterer is not too large and the frequency not too high [*Born and Wolf*, 1980; *Nieto-Vesperinas*, 1991]. However, in many low-frequency geophysical applications, moderate- and high-conductivity contrasts cause both the amplitude and phase of the internal electric field to differ greatly from background values.

The Born approximation is also popular in inverse scattering since it renders the scattering linear with respect to the material properties. When the background medium is homogeneous, the inverse problem can often be solved analytically in a form that is easy to compute [*Oristaglio*, 1989]. Limitations of the Born approximation in a homogeneous background medium can be ameliorated by an iterative approach, where the background medium is updated at each iteration and the distorted-wave Born approximation is used [*Habashy et al.*, 1986]. This approach, however, does not always converge rapidly, particularly at high frequencies and for large scatterers. In electromagnetic problems, it is also less effective for transverse magnetic (TM) polarization than for transverse electric (TE) polarization problems [*Habashy et al.*, 1986, 1990].

Related to the Born approximations is the Rytov approximation which assumes a particular functional form for the field (in terms of the exponential of a complex phase function) before linearizing the scattering problem. The Rytov approximation or transformation is widely used in problems where the length scale of fluctuation is large compared to the wavelength, since its exponential representation is thought to be more representative of wave propagation than the algebraic series representation of the Born approach.

In this paper we show that certain modifications of the Born and Rytov approximations can improve their accuracy dramatically. We present new and relatively simple approximations for the internal electric field which largely account for the full scattering. We illustrate these approximations using the electromagnetic response of a spherical scatterer. Results for the new approximations are much better than the Born and Rytov approximations for conductivity contrasts over several orders of magnitude. These new approximations are generally much faster to compute than the full forward problem and are almost as efficient as the Born or Rytov approximations. The new approximations should have wide applicability both for inverse and forward scattering problems in electromagnetics. Distorted-wave Born or Rytov algorithms will be greatly enhanced, not only in terms of speed and accuracy but also in their range of applicability.

The formulation outlined in this paper for the spherical geometry can be generalized to geometries such as rectan-

Paper number 92JB02324.
0148-0227/93/92JB-02324$05.00

gular parallelepiped, rectangular cylinders, etc. Complex models can be constructed using these simple building blocks, i.e., rectangular prisms or cells of appropriate size. Furthermore, interactions between cells out to an appropriate distance can be readily incorporated by this formulation.

The general concept may also be readily applied to scattering problems in other fields such as quantum mechanics, optics, ultrasonics and seismology.

THE BORN APPROXIMATION IN ELECTROMAGNETICS

This section develops the integral equation for electromagnetic scattering that form the basis for the Born and Rytov approximations. In formulating the problem as an integral equation, one assumes that the scatterer or object (of support V_s) is embedded inside a background medium, which is not necessarily homogeneous. Scattering from the object is described by a volume distribution of currents induced inside the scatterer. The wave equation corresponding to this representation of the electric field (in nonmagnetic media and with an $e^{-i\omega t}$ time dependence) is

$$\nabla \times \nabla \times \mathbf{E}(\mathbf{r}) - k_b^2 \mathbf{E}(\mathbf{r}) = Q(\mathbf{r})\mathbf{E}(\mathbf{r}) + i\omega\mu_0 \mathbf{J}_s(\mathbf{r}) - \nabla \times \mathbf{M}_s(\mathbf{r}), \quad (1)$$

where the wavenumber k_b of the background medium is given by

$$k_b^2 = i\omega\mu_0\sigma_b' + \omega^2\mu_0\varepsilon_b, \quad (2)$$

and $Q(\mathbf{r})$ is the change in the material properties from the background medium,

$$Q(\mathbf{r}) = i\omega\mu_0[\sigma'(\mathbf{r}) - \sigma_b'] + \omega^2\mu_0[\varepsilon(\mathbf{r}) - \varepsilon_b] = i\omega\mu_0[\sigma(\mathbf{r}) - \sigma_b] = i\omega\mu_0\Delta\sigma(\mathbf{r}). \quad (3)$$

In these equations, $\mathbf{J}_s(\mathbf{r})$ and $\mathbf{M}_s(\mathbf{r})$ are the impressed electric and magnetic sources, $\varepsilon(\mathbf{r})$ and $\sigma'(\mathbf{r})$ are the permittivity and conductivity distributions, while ε_b and σ_b' are the background dielectric permittivity and electrical conductivity. In the second part of equation (3), $\sigma(\mathbf{r})$ and σ_b are the complex conductivities which include the effects of displacement currents.

The solution of equation (1) can be expressed with a dyadic Green's function which is governed by the appropriate boundary conditions and satisfies the equation

$$\nabla \times \nabla \times \bar{\bar{G}}(\mathbf{r}, \mathbf{r}') - k_b^2 \bar{\bar{G}}(\mathbf{r}, \mathbf{r}') = \bar{\bar{I}}\delta(\mathbf{r} - \mathbf{r}'), \quad (4)$$

where $\bar{\bar{I}}$ is the identity dyadic.

For a homogeneous background, the solution to equation (4) is [*Kong*, 1986]

$$\bar{\bar{G}}(\mathbf{r}, \mathbf{r}') = \left[\bar{\bar{I}} + \frac{1}{k_b^2}\nabla\nabla\right] g(\mathbf{r}, \mathbf{r}'), \quad (5)$$

where $g(\mathbf{r}, \mathbf{r}')$ is the scalar Green's function which satisfies

$$\nabla^2 g(\mathbf{r}, \mathbf{r}') + k_b^2 g(\mathbf{r}, \mathbf{r}') = -\delta(\mathbf{r} - \mathbf{r}'), \quad (6a)$$

and is given by

$$g(\mathbf{r}, \mathbf{r}') = \frac{e^{ik_b|\mathbf{r} - \mathbf{r}'|}}{4\pi|\mathbf{r} - \mathbf{r}'|}. \quad (6b)$$

Thus the solution of equation (1) is given by [*Kong*, 1986; *Yaghjian*, 1980]

$$\mathbf{E}(\mathbf{r}) = \mathbf{E}_b(\mathbf{r}) + \int_{V_s} d\mathbf{r}' \bar{\bar{G}}(\mathbf{r}, \mathbf{r}') \cdot Q(\mathbf{r}')\mathbf{E}(\mathbf{r}'), \quad \mathbf{r} \notin V_s \quad (7a)$$

$$\mathbf{E}(\mathbf{r}) = \mathbf{E}_b(\mathbf{r}) + \left(\bar{\bar{I}} + \frac{1}{k_b^2}\nabla\nabla\right) \cdot \int_{V_s} d\mathbf{r}'\, g(\mathbf{r}, \mathbf{r}')Q(\mathbf{r}')\mathbf{E}(\mathbf{r}'), \quad \mathbf{r} \in V_s \quad (7b)$$

where V_s is the support of $Q(\mathbf{r})$. The response of the impressed sources in the background medium, $\mathbf{E}_b(\mathbf{r})$, is the solution of the wave equation

$$\nabla \times \nabla \times \mathbf{E}_b(\mathbf{r}) - k_b^2 \mathbf{E}_b(\mathbf{r}) = i\omega\mu_0 \mathbf{J}_s(\mathbf{r}) - \nabla \times \mathbf{M}_s(\mathbf{r}). \quad (8)$$

Care must be exercised in using equation (7*b*) when commuting the $\nabla\nabla$ operator with the integral operator because of the nonintegrable singularity of the derivatives of the scalar Green's function $g(\mathbf{r}, \mathbf{r}')$ at $\mathbf{r}' = \mathbf{r}$.

Equation (7), for both internal and external points, can be recast in a form that separates the scattered field into components which we term inductive (due to the vector potential) and galvanic (due to the scalar potential) [*Jackson*, 1975]:

$$\mathbf{E}(\mathbf{r}) = \mathbf{E}_b(\mathbf{r}) + \int_{V_s} d\mathbf{r}'\, g(\mathbf{r}, \mathbf{r}')Q(\mathbf{r}')\mathbf{E}(\mathbf{r}') + \frac{1}{k_b^2}\nabla\nabla \cdot \int_{V_s} d\mathbf{r}'\, g(\mathbf{r}, \mathbf{r}')Q(\mathbf{r}')\mathbf{E}(\mathbf{r}'). \quad (9)$$

Any one of equations (7*a*), (7*b*), or (9) can be employed as the basic integral equation of electromagnetic scattering. In these equations, the total field is represented as the sum of the background field $\mathbf{E}_b(\mathbf{r})$ and the scattered field (the integral terms). The scattered field is generated by the scattering currents (and charges) induced inside the scatterer by the interaction of the total electric field $\mathbf{E}(\mathbf{r})$ with material variation $Q(\mathbf{r})$. These equations are nonlinear in $Q(\mathbf{r})$ since the total field, which multiplies $Q(\mathbf{r})$, also depends nonlinearly on $Q(\mathbf{r})$.

Under the Born approximation the total electric field in the integral terms is approximated by the background field. This approximation gives a representation of $\mathbf{E}(\mathbf{r})$ that is linear in $Q(\mathbf{r})$. In fact, the Born approximation is the first term in a solution of equation (7) by successive iteration. The full series is called the Born or Neumann series. The convergence of this series expansion is of fundamental importance, since such expansions in perturbation series are generally either divergent or very slowly convergent for large contrasts. To analyze the convergence, we will use a dimensionless contrast defined as

$$\delta = \frac{1}{|k_b^2|} \max\{|Q(\mathbf{r})|\}, \quad (10)$$

which simplifies to $(\sigma'_{\max} - \sigma_b')/\sigma_b'$ when displacement currents are neglected. If one applies the Born approximation to equation (9) one can show that, in the low-frequency

limit, the strength of the induction term in the scattered field is determined by $|k_b^2|D^2\delta$ (where D is the upper bound of the distance of any two points belonging to V_s), whereas the strength of the galvanic term is determined by δ [*Habashy et al.*, 1986]. Thus the induction term can be made arbitrarily small by either lowering the frequency (lowering k_b) for a given contrast δ or by lowering the contrast δ for a given frequency. On the other hand, the galvanic term can only be made small by lowering the contrast δ. Thus, at a frequency that is sufficiently low, the sum of the inductive terms in the Born series can converge even for large contrasts. The galvanic terms, however, will only converge when the conductivity contrast δ is small; that is, the background medium must have a conductivity distribution close to that of the scatterer. This requirement can be met in many cases only by using a complex background medium. If the background medium is complex, it can be difficult or costly to compute both the background field and the Green's function in equation (7). This greatly limits the usefulness of the Born approximation.

In summary, the fundamental difference between the induction and galvanic terms lie in the degree of nonlinearity associated with each term. In equation (9) both the induction and galvanic terms are nonlinear in the conductivity distribution of the scatterer $Q(\mathbf{r})$, because the total internal electric field also depends nonlinearly on $Q(\mathbf{r})$. However, the induction term is almost linear when $|k_b^2|D^2\delta$ is small, whereas the galvanic term is highly nonlinear (unless δ is small). Thus the Born approximation, which linearizes the problem in $Q(\mathbf{r})$, is expected to be much better for the induction term than for the galvanic.

In general, the Born approximation is a weak scatterer approximation that is accurate when the difference between the internal and background electric fields are small. This restriction limits the domain of usefulness of the Born approximation. However, in cases where the scattered field consists only of inductive effects, the Born series should work well at low frequencies and will not require many terms to converge.

The Rytov Approximation in Electromagnetics

Another commonly used approximation for scattering problems is the Rytov approximation [*Keller*, 1969; *Oristaglio*, 1985; *Sancer and Varvatsis*, 1970]. In this section we review the Rytov approximation in electromagnetics and compare it to the Born approximation.

The vector wave equation for the electric field can be rewritten as

$$\nabla^2\mathbf{E} + k^2\mathbf{E} - \nabla\{\nabla\cdot\mathbf{E}\} = -i\omega\mu_0\mathbf{J}_s + \nabla\times\mathbf{M}_s, \quad (11)$$

with

$$k^2 = i\omega\mu_0\sigma(\mathbf{r}) = i\omega\mu_0\sigma'(\mathbf{r}) + \omega^2\mu_0\varepsilon(\mathbf{r}). \quad (12)$$

where k is the wavenumber of the scatterer. From the equation for the conservation of charge, we have

$$\nabla\cdot\mathbf{E} = -\frac{\nabla\sigma}{\sigma}\cdot\mathbf{E} - \frac{1}{\sigma}\nabla\cdot\mathbf{J}_s. \quad (13)$$

Hence the vector wave equation for the electric field can be written as

$$\nabla^2\mathbf{E} + k^2\mathbf{E} + \nabla\left\{\frac{\nabla\sigma}{\sigma}\cdot\mathbf{E}\right\} = -i\omega\mu_0\mathbf{J}_s - \nabla\left\{\frac{1}{\sigma}\nabla\cdot\mathbf{J}_s\right\} + \nabla\times\mathbf{M}_s. \quad (14)$$

The third term in the left-hand side of equation (14) is commonly referred to as the polarization term, since it represents the effect of the polarization charges in the medium. At high frequencies, i.e., when the wavelength λ is small compared to the characteristic dimension D of the scatterer and when $\sigma(\mathbf{r})$ is smoothly varying, the polarization term is of the order of $|\mathbf{E}|/D\lambda$, which is small compared to the second term of the left-hand side of equation (14), which is of the order of $|\mathbf{E}/\lambda^2$. Thus, when the wavelength is much smaller than the scale size of the scatterer, the polarization term can be neglected and the vector wave equation reduces to uncoupled scalar equations for each cartesian component of $\mathbf{E}(\mathbf{r})$ [*Tatarskii*, 1971]. Furthermore, the third term in the left-hand side of equation (14) does not contribute to the scattered field outside the support of the scatterer since it can be shown that it represents a "nonradiating" current source [*Lindell*, 1988]. The source-free wave equation governing an arbitrary cartesian component of the electric field is

$$\nabla^2 E(\mathbf{r}) + k^2 E(\mathbf{r}) = 0. \quad (15)$$

The Rytov transformation consists of representing the solution of equation (15) in the form

$$E(\mathbf{r}) = E_b(\mathbf{r})e^{\psi(\mathbf{r})}, \quad (16)$$

and developing a series expansion for the complex phase function $\psi(\mathbf{r})$. The Rytov approximation is used in problems where the length scale of fluctuation is large compared to the wavelength, since its exponential representation is more representative of wave propagation than the algebraic series representation of the Born approach. Substituting equation (16) in equation (15) and rearranging terms [*Kak and Slaney*, 1988; *Nieto-Vesperinas*, 1991; *Sobczyk*, 1985] gives

$$(\nabla^2 + k_b^2)(E_b\psi) = -[(\nabla\psi)^2 + Q(\mathbf{r})]E_b. \quad (17)$$

Equation (17) is nonlinear in ψ but is linearized under the Rytov approximation by neglecting the first term on the right-hand side of equation (17) relative to the second term

$$(\nabla^2 + k_b^2)(E_b\psi) = -Q(\mathbf{r})E_b. \quad (18)$$

On the other hand, the Born approximation $E^{(B)}(\mathbf{r})$ of equation (15), cast as a differential equation, is

$$(\nabla^2 + k_b^2)E^{(B)} = -Q(\mathbf{r})E_b. \quad (19)$$

Thus the phase function ψ in the Rytov approximation is related to the Born approximation for the scattered wave field, $E^{(B)}(\mathbf{r})$, by

$$\psi(\mathbf{r}) = E^{(B)}(\mathbf{r})/E_b(\mathbf{r}). \quad (20)$$

Clearly, when $|E^{(B)}/E_b| \ll 1$, the Rytov approximation reduces to the Born approximation. Since equation (17) is exact, the Rytov approximation is valid when

$$|Q| \gg |\nabla\psi|^2. \quad (21)$$

In the previous section, we analyzed the Born approximation in the low-frequency limit. In the high-frequency limit, the Born approximation is accurate when the change in the phase between the wave propagating through the scatterer and the background field is much less than unity [*Kak and Slaney*, 1988; *Sobczyk*, 1985]. Thus, in the high frequency limit, the condition for good accuracy of the Born approximation can be expressed mathematically as

$$|\psi| \sim |kD - k_b D| \leq |k_b| D[(1+\delta)^{1/2} - 1] \ll 1, \qquad (22)$$

which simplifies to

$$|k_b| D\delta \ll 1. \qquad (23)$$

Comparing equations (21) and (23) it is clear that in contrast to the Born approximation, the size of the scatterer is not a factor in determining the accuracy of the Rytov approximation. The gradient of ψ is just the change per unit distance in the complex phase of the wavefield as given by equation (16). Thus it is the change in the phase ψ that is important in determining the accuracy of the Rytov approximation and not the total phase through the scatterer as with the Born approximation.

In the high-frequency limit,

$$\psi(\mathbf{r}) \sim i\{\mathbf{k} - \mathbf{k_b}\} \cdot \mathbf{r}, \qquad (24)$$

and hence

$$|\nabla\psi| \sim |\mathbf{k} - \mathbf{k_b}| = |k_b| \left| \left(1 + \frac{Q}{k_b^2}\right)^{1/2} - 1 \right|. \qquad (25)$$

Substituting equation (25) in equation (21) gives

$$\left| \left(1 + \frac{Q}{k_b^2}\right)^{1/2} - 1 \right| \ll \left| \frac{Q}{k_b^2} \right|^{1/2}, \qquad (26a)$$

which simplifies to

$$|Q/k_b^2|^{1/2} \ll 1. \qquad (26b)$$

Hence the condition for the good accuracy of the Rytov approximation becomes

$$\delta \ll 1. \qquad (27)$$

Thus, in the high-frequency regime, the Rytov approximation is accurate only for small contrasts between the scatterers and the background medium. Moreover, comparing equations (23) and (27), one concludes that for a given contrast, the Rytov approximation is accurate over a larger range of scatterer sizes than is the Born approximation. A schematic diagram showing the range of accuracy of the Born and Rytov approximations is shown in Figure 1.

In the next sections we describe new approximations for the scattered electric field which are similar in spirit to the Born and Rytov approximations but are accurate over a much wider range of frequencies and contrasts in physical properties.

A Localized Nonlinear Approximation for Internal Electric Field

Consider again equation (7), the basic integral equation of electromagnetic scattering. For observation points ($\mathbf{r} \in V_s$) inside the scatterer, one must be careful in defining the volume integral because of the singularity of the Dyadic Green's function. For interior points, equation (7) can be rewritten as

$$\mathbf{E}(\mathbf{r}) = \mathbf{E_b}(\mathbf{r}) + \left[\left(\bar{\bar{I}} + \frac{1}{k_b^2} \nabla\nabla \right) \int_{V_s} d\mathbf{r}'\, g(\mathbf{r}, \mathbf{r}') Q(\mathbf{r}') \right] \cdot \mathbf{E}(\mathbf{r}) + \int_{V_s} d\mathbf{r}'\, \bar{\bar{G}}(\mathbf{r}, \mathbf{r}') Q(\mathbf{r}') [\mathbf{E}(\mathbf{r}') - \mathbf{E}(\mathbf{r})]. \qquad (28)$$

The terms on the right-hand side involving $\mathbf{E}(\mathbf{r})$ cancel in the above equation, when interpreted properly according to equation (7). Thus equation (28) is equivalent to equation (7), but the singularities in the integrands are now integrable as explicitly expressed. Indeed, the integrand of the last integral of equation (28) is now integrable since $\mathbf{E}(\mathbf{r}') - \mathbf{E}(\mathbf{r})$ vanishes as $\mathbf{r}' \to \mathbf{r}$ where $\bar{\bar{G}}(\mathbf{r}, \mathbf{r}')$ is singular.

Further algebraic manipulation of equation (28) gives the following integral equation of the internal electric field:

$$\mathbf{E}(\mathbf{r}) = \bar{\bar{\Gamma}}(\mathbf{r}) \cdot \left[\mathbf{E_b}(\mathbf{r}) + \int_{V_s} d\mathbf{r}'\, \bar{\bar{G}}(\mathbf{r}, \mathbf{r}') \cdot Q(\mathbf{r}')\{\mathbf{E}(\mathbf{r}') - \mathbf{E}(\mathbf{r})\} \right], \qquad \mathbf{r} \in V_s \qquad (29)$$

where $\bar{\bar{\Gamma}}(\mathbf{r})$ is a dyadic which we call the depolarization tensor and is given by

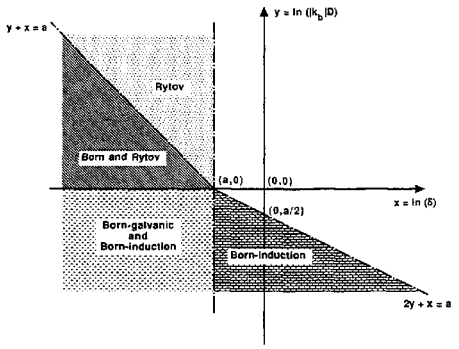

Fig. 1. The range of validity of various approximations. The abscissa is $x = \ln(\delta)$, where δ is the contrast in material properties (defined in equation (10)). The ordinate is the logarithm of the product of the background wavenumber and a characteristic dimension of the scatterer. The parameter a is a negative number such that $e^a \ll 1$. The Rytov approximation is valid in the range $|k_b|D > 1$ and $\delta \ll 1$. The Born approximation is valid in the range $|k_b|D\delta \ll 1$ in the high-frequency regime ($|k_b|D > 1$). In the low-frequency regime ($|k_b|D < 1$), the galvanic part of the scattered field is valid under the Born approximation in the range $\delta \ll 1$, whereas the induction part is valid in the range $|k_b|^2 D^2 \delta \ll 1$. The new approximations introduced in this paper have a range of validity which extends beyond the shaded zones and into the unshaded area.

$$\bar{\bar{\Gamma}}(\mathbf{r}) = \left[\bar{\bar{I}} - \left(\bar{\bar{I}} - \frac{1}{k_b^2}\nabla\nabla\right)\int_{V_s} d\mathbf{r}'\, g(\mathbf{r}, \mathbf{r}')Q(\mathbf{r}')\right]^{-1}. \tag{30}$$

Under the Born approximation, the electric field in the integral over the volume of the scatterer is simply approximated by the background electric field. An alternative approximation for the electric field in the integral of the electric field is given by the first term in equation (29)

$$\mathbf{E}(\mathbf{r}) \approx \bar{\bar{\Gamma}}(\mathbf{r}) \cdot \mathbf{E}_b(\mathbf{r}), \qquad \mathbf{r} \in V_s, \tag{31}$$

An argument in favor of this approximation is as follows: from the singular nature of $\bar{\bar{G}}(\mathbf{r}, \mathbf{r}')$ at $\mathbf{r}' = \mathbf{r}$ one may expect that the dominant contribution to the integral in equation (7) comes from points in the vicinity of $\mathbf{r}' = \mathbf{r}$. If the internal electric field $\mathbf{E}(\mathbf{r}')$ is approximated by its value at $\mathbf{r}' = \mathbf{r}$, the second term in equation (28) gives the full approximation of the scattered field, with an error given by the third term. This approximation is particularly appropriate if the internal electric field is a smoothly varying function of position, since the approximation in equation (31) assumes that

$$|\mathbf{E}_b(\mathbf{r})| \gg \left|\int_{V_s} d\mathbf{r}'\, \bar{\bar{G}}(\mathbf{r}, \mathbf{r}') \cdot Q(\mathbf{r}')\{\mathbf{E}(\mathbf{r}') - \mathbf{E}(\mathbf{r})\}\right|, \qquad \mathbf{r} \in V_s. \tag{32}$$

The right hand side of the above inequality can be expected to be small because $\mathbf{E}(\mathbf{r}') - \mathbf{E}(\mathbf{r})$ is zero where $\bar{\bar{G}}(\mathbf{r}, \mathbf{r}')$ is singular, i.e, at $\mathbf{r}' = \mathbf{r}$. Hence the accuracy of the approximation depends on $\bar{\bar{G}}(\mathbf{r}, \mathbf{r}')$ falling off sufficiently rapidly as $\mathbf{r}'$ moves away from $\mathbf{r}$ that variations in the internal electric field from its value at $\mathbf{r}$ are small. We call the approximation given by equation (31) the localized nonlinear (LN) approximation. The approximation depends nonlinearly on $Q(\mathbf{r})$.

If $Q \neq 0$, then $\bar{\bar{\Gamma}}(\mathbf{r})$ has a DC limit $\bar{\bar{\Gamma}}_0(\mathbf{r})$ with elements entirely real and different from $\bar{\bar{I}}$. In this DC limit, equation (31) becomes

$$\mathbf{E}(\mathbf{r}) \approx \bar{\bar{\Gamma}}_0(\mathbf{r}) \cdot \mathbf{E}_b(\mathbf{r}), \qquad \mathbf{r} \in V_s. \tag{33}$$

which we call the static localized nonlinear (SLN) approximation. It accounts for the difference in amplitude of the total internal field from background field caused by charge accumulations on the boundaries of the scatterer.

Under the localized nonlinear (LN) approximation, the electric field at points outside V_s is given by

$$\mathbf{E}(\mathbf{r}) \approx \mathbf{E}_b(\mathbf{r}) + \int_{V_s} d\mathbf{r}'\, \bar{\bar{G}}(\mathbf{r}, \mathbf{r}') \cdot Q(\mathbf{r}')\bar{\bar{\Gamma}}(\mathbf{r}') \cdot E_b(\mathbf{r}'), \qquad \mathbf{r} \notin V_s \tag{34}$$

and the magnetic field by

$$\mathbf{H}(\mathbf{r}) = \frac{1}{i\omega\mu_0}\nabla \times \mathbf{E}(\mathbf{r}) \approx \mathbf{H}_b(\mathbf{r}) + \frac{1}{i\omega\mu_0} \cdot \int_{V_s} d\mathbf{r}'\, [\nabla g(\mathbf{r}, \mathbf{r}')] \times Q(\mathbf{r}')\bar{\bar{\Gamma}}(\mathbf{r}') \cdot \mathbf{E}_b(\mathbf{r}'). \tag{35}$$

For the simpler static localized nonlinear (SLN) approximation, $\bar{\bar{\Gamma}}(\mathbf{r})$ is replaced by $\bar{\bar{\Gamma}}_0(\mathbf{r})$ in equations (34) and (35).

Expanding the depolarization tensor $\bar{\bar{\Gamma}}(\mathbf{r})$ in equations (34) and (35) in a Taylor series expansion in Q shows that the LN approximation accounts for some of the multiple scattering within the scatterer. This is to be compared to the standard Born approximation, the first-order term in the complete Neumann (or Born) series [*Newton*, 1966], which ignores all multiple scattering.

Also, when applied to a conducting inhomogeneous scatterer embedded in an insulating background, the Born approximation may diverge in the zero frequency limit depending on the source excitation, since

$$Q(\mathbf{r})/k_b^2 \to i\sigma'(\mathbf{r})/\omega\varepsilon_b \to \infty, \qquad \omega \to 0. \tag{36}$$

This is a consequence of approximating the scattering currents inside the scatterer by those induced by the background field,

$$\mathbf{J}_{sc}(\mathbf{r}) = \{\sigma'(\mathbf{r}) - i\omega[\varepsilon(\mathbf{r}) - \varepsilon_b]\}\mathbf{E}(\mathbf{r}) \approx \{\sigma'(\mathbf{r}) - i\omega[\varepsilon(\mathbf{r}) - \varepsilon_b]\}\mathbf{E}_b(\mathbf{r}) \tag{37}$$

which gives rise to a charge density

$$\rho_{sc}(\mathbf{r}) = \frac{1}{i\omega}\nabla \cdot \mathbf{J}_{sc}(\mathbf{r}) \approx \frac{1}{i\omega}\{\nabla(\sigma'(\mathbf{r}) - i\omega\varepsilon(\mathbf{r})]\} \cdot \mathbf{E}_b(\mathbf{r}) \tag{38}$$

that can diverge in the low-frequency limit depending on the source excitation, since

$$\rho_{sc}(\mathbf{r}) \approx \frac{\nabla\sigma'(\mathbf{r})}{i\omega} \cdot \mathbf{E}_b(\mathbf{r}) \to \infty, \qquad \omega \to 0. \tag{39}$$

In the low-frequency regime, the background field is a very poor estimate of the internal fields of a conducting scatterer in an insulating background medium. This divergent behavior of the Born approximation is alleviated by the newly developed LN approximation, which produces a finite contribution from the surface charges to the scattered field in the low-frequency limit. Thus unlike the Born approximation, these new estimators should be applicable to applications where the host media is extremely resistive.

A Localized Nonlinear Rytov Approximation

An arbitrary component of the electric or magnetic field can always be represented as the sum of a background field and a scattered field,

$$F(\mathbf{r}) = F_b(\mathbf{r}) - F_s(\mathbf{r}). \tag{40}$$

As described earlier, the Rytov transformation consists of representing the wavefield component $F(\mathbf{r})$ in the following form:

$$F(\mathbf{r}) = F_b(\mathbf{r})e^{\psi(\mathbf{r})}, \tag{41}$$

and developing a series expansion for the complex phase function $\psi(\mathbf{r})$. Comparing equations (40) and (41), gives

$$\psi(\mathbf{r}) = \ln\left\{1 + \frac{F_s(\mathbf{r})}{F_b(\mathbf{r})}\right\}. \tag{42}$$

Assuming $|F_s/F_b| < 1$, invoking the Taylor series expansion of the logarithmic function, and retaining only the first term gives the following approximate representation of $\psi(\mathbf{r})$

$$\psi(\mathbf{r}) \approx \frac{F_s(\mathbf{r})}{F_b(\mathbf{r})}, \tag{43}$$

and hence

$$F(\mathbf{r}) \approx F_b(\mathbf{r}) \exp\left\{\frac{F_s(\mathbf{r})}{F_b(\mathbf{r})}\right\}. \tag{44}$$

Replacing $F_s(\mathbf{r})$ by its first-order Born approximation, $F_s^{(B)}(\mathbf{r})$, we obtain the standard Rytov approximation denoted by $F_R(\mathbf{r})$

$$F_R(\mathbf{r}) = F_b(\mathbf{r}) \exp\left\{\frac{F_s^{(B)}(\mathbf{r})}{F_b(\mathbf{r})}\right\}. \tag{45}$$

Replacing $F_s(\mathbf{r})$ by its static localized nonlinear (SLN) approximation $F_s^{(SLN)}(\mathbf{r})$ gives a new approximation, which we call the static localized nonlinear Rytov (SLNR) approximation, denoted by $F_{SLNR}(\mathbf{r})$

$$F_{SLNR}(\mathbf{r}) = F_b(\mathbf{r}) \exp\left\{\frac{F_s^{(SLN)}(\mathbf{r})}{F_b(\mathbf{r})}\right\}. \tag{46}$$

Finally, replacing $F_s(\mathbf{r})$ by its localized nonlinear (LN) approximation $F_s^{(LN)}(\mathbf{r})$ gives another new approximation, which we call the localized nonlinear Rytov (LNR) approximation, denoted by $F_{LNR}(\mathbf{r})$

$$F_{LNR}(\mathbf{r}) = F_b(\mathbf{r}) \exp\left\{\frac{F_s^{(LN)}(\mathbf{r})}{F_b(\mathbf{r})}\right\}. \tag{47}$$

The accuracy of all of these approximations is tested numerically in the next two sections. We show that these approximations agree well with exact computations, even in the case when the condition $|F_s/F_b| < 1$ is not satisfied.

Application to a Spherical Scatterer

The approximations developed in the previous section depend on the geometry of the scatterer. To illustrate the computation of these approximations and also to demonstrate their improvements over the Born and Rytov approximations, we study in detail a uniformly conducting spherical scatterer, of complex conductivity σ_s, embedded in a uniform whole space, of complex conductivity σ_b.

In Appendix A, we explicitly express the internal electric field, in the LN approximation, in terms of the background field and functions which are solely dependent on geometry, frequency, and the conductivity of the background medium. The expression for the internal electric field in the LN approximation is given explicitly as

$$\mathbf{E}(\mathbf{r}) = \left(1 - \frac{\Delta\sigma}{\sigma_b} h(\mathbf{r})\right)^{-1} \cdot \left[\mathbf{E_b}(\mathbf{r}) + \frac{\Delta\sigma}{\sigma_b} p(\mathbf{r}) \frac{\hat{\mathbf{r}} \cdot \mathbf{E_b}(\mathbf{r})}{1 - (\Delta\sigma/\sigma_b)s(\mathbf{r})} \hat{\mathbf{r}}\right], \quad \mathbf{r} \in V_s. \tag{48}$$

where

$$\Delta\sigma = \sigma_s - \sigma_b, \tag{49a}$$

$$\sigma_s = \sigma'_s - i\omega\varepsilon_s, \tag{49b}$$

$$\sigma_b = \sigma'_b - i\omega\varepsilon_b. \tag{49c}$$

with the prime indicating real part, and

$$h(\mathbf{r}) = k_b^2 f(\mathbf{r}) + \frac{f'(\mathbf{r})}{r} = -1 + \frac{\psi(k_b a)}{k_b r} \cdot \left[\sin(k_b r) + \frac{\cos(k_b r)}{k_b r} - \frac{\sin(k_b r)}{(k_b r)^2}\right] \tag{50a}$$

$$p(\mathbf{r}) = f''(\mathbf{r}) - \frac{f'(\mathbf{r})}{r} = -\frac{\psi(k_b a)}{k_b r} \cdot \left[\sin(k_b r) + 3\frac{\cos(k_b r)}{k_b r} - 3\frac{\sin(k_b r)}{(k_b r)^2}\right] \tag{50b}$$

$$s(\mathbf{r}) = h(\mathbf{r}) + p(\mathbf{r}) \tag{50c}$$

$$f(\mathbf{r}) = \int_{V_s} d\mathbf{r}'\, g(\mathbf{r}, \mathbf{r}') = \frac{1}{k_b^2}\left[-1 + \psi(k_b a)\frac{\sin(k_b r)}{k_b r}\right] \tag{50d}$$

$$\psi(k_b a) = (1 - ik_b a)e^{ik_b a}. \tag{51}$$

The primes on the function f in equation (50) denote differentiation with respect to the argument. The low-frequency asymptotes of these expressions, when $|k_b a| \ll 1$, are

$$h(\mathbf{r}) \approx -\tfrac{1}{3} + \tfrac{1}{3}(k_b a)^2 - \frac{2}{15}(k_b r)^2 \tag{52a}$$

$$p(\mathbf{r}) \approx \tfrac{1}{15}(k_b r)^2. \tag{52b}$$

In the DC limit, we have

$$h(\mathbf{r}) \to -\tfrac{1}{3} \tag{53a}$$

$$p(\mathbf{r}) \to 0 \tag{53b}$$

and therefore from equations (A2) and (A10) of Appendix A, we obtain

$$\bar{\bar{\Gamma}}_0(\mathbf{r}) = \left(1 + \frac{1}{3}\frac{\Delta\sigma}{\sigma_b}\right)^{-1} \bar{\bar{I}} = \left(\frac{3\sigma_b}{\sigma + 2\sigma_b}\right)\bar{\bar{I}}. \tag{54}$$

The factor $\frac{1}{3}$ is referred to as the depolarization factor which originally appeared in connection with scattering from a dielectric sphere [*Van Kranendock and Sipe*, 1977; *Yaghjian*, 1980].

From equations (33) and (54) the internal electric field under the SLN approximation is given by

$$\mathbf{E}(\mathbf{r}) \approx \left(\frac{3\sigma_b}{\sigma + 2\sigma_b}\right)\mathbf{E_b}(\mathbf{r}), \qquad \mathbf{r} \in V_s. \tag{55}$$

From equation (48) it is clear that the internal electric field, under the localized nonlinear (LN) approximation, is given by the background field modified by an additive and a multiplicative factor. The additive factor corrects mainly for the phase and slightly for the amplitude. It also estimates

cross-polarization effects due to the scatterer. The multiplicative factor corrects primarily for the amplitude and slightly for the phase. The simpler SLN estimator, with $p(\mathbf{r}) = 0$, is only a multiplicative factor, and thus equation (55) contains no cross-polarization terms.

With the internal electric field estimated by either equation (55) or equation (48), the SLN or the LN approximations to the corresponding external scattered electric and magnetic fields follow from equations (34) and (35). This then allows the computation of the SLNR and LNR approximations from equations (46) and (47), respectively.

For most geophysical applications the fields outside the scatterer are of principle interest. We will examine the accuracy of the approximations derived above for the external scattered electric and magnetic fields and also the internal total electric field (Appendix C) by comparing the estimated solutions with an exact solution for a sphere over a wide range of conductivity contrasts between the scatterer and the background medium.

Comparison of Approximations With Exact Solutions: External Scattered Magnetic Field

Formulation of the depolarization tensor for a spherical scatterer in a dipolar field is straightforward. The main reason for using this configuration is that we are able to compare the approximations to an accurate benchmark solution for full-wave scattering from a sphere in a conducting background (R. W. Groom and T. M. Habashy, manuscript in preparation, 1992) for an arbitrarily positioned and oriented magnetic dipole. The formulations used to calculate the estimated scattered fields are given in Appendix B. Figure 2 illustrates the model, coordinate system, and symbols for the models used.

In most geophysical applications the magnetic field is of primary interest. Thus we begin our examination of the accuracy of the new estimators as compared to the Born and Rytov approximations by computing solutions for the scattered magnetic field $\mathbf{H}_s(\mathbf{r})$ external to the scatterer. In our first example (Figure 3), the source is situated at $Tx = (r, \theta, \phi) = (10, 90°, -90°)$ and the receiver at $Rx = (10, 45°, 0°)$. Initially, we begin with a small sphere ($R = 1$ m), as the Born approximation is expected to be most accurate for small scatterers. The receiver Rx is in the far field relative to the sphere radius and the primary fields are relatively uniform over the scatterer. In addition, we use a moderately low frequency, $f = 100$ Hz, primarily to examine the ability of the static estimator (SLN) to improve the approximations of the amplitude of the scattered fields. Figure 3 compares the true solution for H_y to the various approximations as a function of the conductivity ratio between the sphere and the background. At this receiver location, H_y is the dominant scattered magnetic field component, and at this frequency it is essentially in-phase with the primary field. The background conductivity is kept constant at 0.1 S/m, while the conductivity of the scatterer is varied.

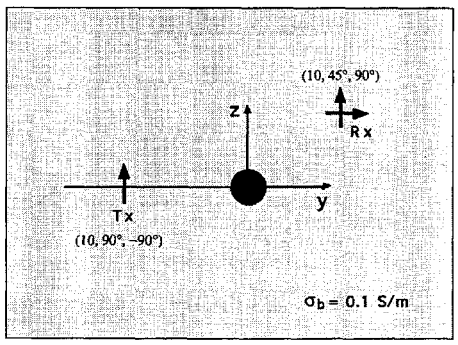

Fig. 2. The generic model with coordinate system. The sphere is centered at the origin.

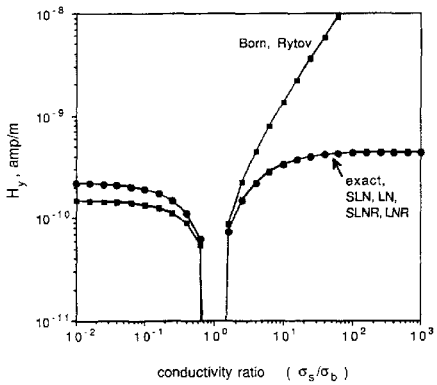

Fig. 3. Comparison of the y component amplitude of the scattered magnetic field for varying conductivity of a small sphere in a uniform (0.1 S/m) background. The frequency of excitation is 100 Hz and the sphere radius is 1 m. The Tx and Rx are fixed at $Tx = (r, \theta, \phi) = (10, 90°, -90°)$ and $Rx = (r, \theta, \phi) = (10, 45°, 0°)$. All four new approximations provide excellent estimates of the response over the entire range of conductivity contrast.

The SLN static approximation provides very good estimates of the true solution over 5 orders of magnitude of conductivity contrast. At this frequency, the scattered field amplitude and the amplitudes of the scattered field approximations are small compared to the background. Thus the Rytov extension to the SLN (the SLNR approximation, equation (46)) provides no additional correction, and the Rytov approximation is almost identical to the Born approximation (equation (45)). At this frequency, the full LN and SLN approximations are virtually identical as there are no phase variations within the scatterer relative to the background field. Since the LN and SLN approximations are identical, the SLNR and LNR approximations must necessarily be equivalent.

The Born and Rytov approximations, on the other hand, are inaccurate except when the conductivity contrast δ is extremely small. In particular, both approximations very quickly overestimate the magnitude of the scattered field when the sphere is more conducting than the host. Because the scattering currents induced inside the scatterer are represented by $(\Delta\sigma\mathbf{E}_b)$ for the Born approximation, the scattered magnetic field very quickly becomes proportional to sphere's conductivity. In the exact solution, on the other

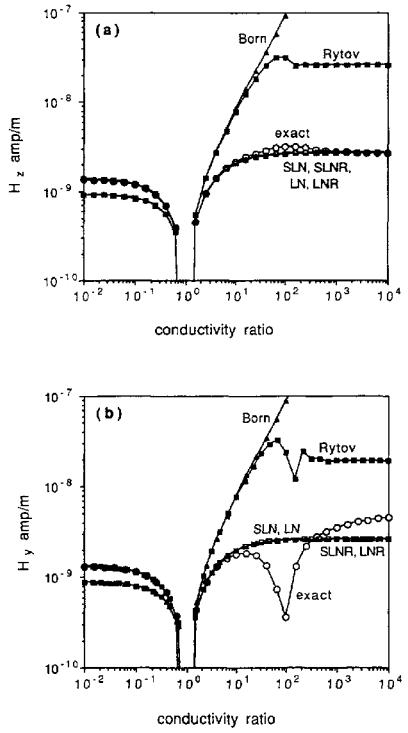

Fig. 4. The amplitude of the scattered magnetic field components (H_z, H_y) plotted as a function of conductivity ratio. The sphere radius is increased to 30 m. The transmitter and receiver locations are $Tx = (r, \theta, \phi) = (100, 90°, -90°)$ and $Rx = (r, \theta, \phi) = (60, 45°, 90°)$. For this sphere size and frequency (100 Hz) there is virtually no difference between the full estimator (LN) and the static estimator (SLN), which give good results for H_y when $\sigma_s/\sigma_b < 20$ and excellent results for H_z at all contrasts.

hand, the internal electric field eventually saturates and the scattered magnetic field does not increase linearly with $\Delta\sigma$. For a resistive sphere, under the Born approximation, the internal scattering currents are soon approximated by $(-\sigma_b \mathbf{E_b})$ as $\sigma \to 0$, and the magnetic field amplitude asymptotes to a value that underestimates the true response.

The second example is a much larger sphere with 30 m radius. The sphere size is now comparable to the distance to the receiver as well as the transmitter. Measured in sphere radii, the transmitter is closer to the sphere (slightly more than 3 radii) and the receiver is also closer (only 2 radii) than in the previous example. There is now a significant scattered H_z field as well as H_y. In Figure 4*a* we plot the amplitude of H_z as given by the true solution (sphere), and the various approximations.

The Born approximation increases in amplitude linearly with conductivity contrast. Because of the corresponding exponential rise in amplitude in the Rytov approximation (equation (45)), the total field estimate approaches a vanishing value for high values of conductivity contrast and hence the scattered field saturates to the negative of the background field (see equations (40) and (45)). The Born and Rytov approximations are only accurate when the conductivity contrast δ is very small. At this relatively low frequency, the amplitudes of the scattered fields are still quite small compared to the background, and therefore there is little difference between the LN and SLN approximations and their Rytov extensions. The frequency is still low enough that there is no appreciable phase difference between the total field and the background field and thus the LN and SLN approximations are equivalent. All four new approximations match the scattered field closely for both conducting and resistive spheres. There is a small but consistent error in the approximations for conductivity ratios around 100. The discrepancy is much larger in the H_y component (Figure 4*b*) for which there is a sharp drop in the true field amplitude for ratios around 100. The scattered H_y amplitude has a minimum just outside the sphere (coinciding with a peak in the scattered H_z amplitude) indicating a rotation of the vector field. The amplitude of the vector scattered field (not shown here) has a slight minimum for a ratio about 80 and then begins to rise again for larger ratios. These characteristics are not predicted by the any of the approximations. In addition, the new approximations underestimate the high conductivity asymptote for the H_y component.

As the sphere size becomes larger or frequencies become higher, all field components of the secondary field $\mathbf{H}_s$ become significant, as does the quadrature scattered field. To study the approximations, we use a normalized residual between the true solution and a given approximation defined as

$$\varepsilon = \frac{\|\hat{\mathbf{H}} - \mathbf{H}_{\text{sphere}}\|}{\|\mathbf{H}_{\text{sphere}}\|} \tag{56}$$

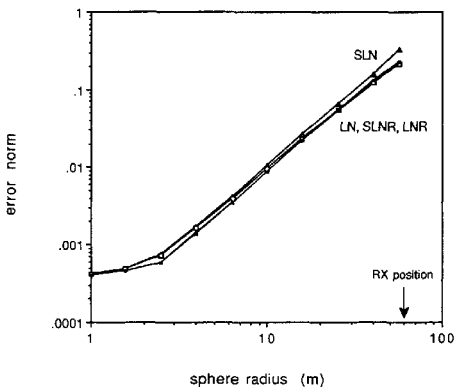

Fig. 5. The residual error norm $\varepsilon = \|\hat{\mathbf{H}} - \mathbf{H}_{\text{sphere}}\|/\|\mathbf{H}_{\text{sphere}}\|$ plotted as a function of sphere radius. The sphere and background conductivities are fixed at 1.0 and 0.1 S/m, respectively, the frequency is 100 Hz, and the Rx and Tx locations are as in Figure 4. The new estimators have errors less than 0.1% for small spheres, rising to between 15% and 25% for a 58 m radius sphere.

where $\hat{\mathbf{H}}$ represents the estimated scattered magnetic field vector and $\|\mathbf{x}\|$ is the Euclidean norm. In Figure 5 we compare the approximations for a fixed frequency, background, and sphere conductivity as the sphere radius is varied. The Rx and Tx positions are as in the second example. The new approximations provide extremely good estimates for small scatterers (error less than 0.1%), but as the sphere radius becomes larger the approximations become somewhat poorer. The LN, SLNR, and LNR approximations estimate the scattered field most accurately, giving an error of about 20% when the observation point is just outside the sphere (the sphere radius is 58 m). It should be noted that as the sphere size increases, the Rx position becomes progressively closer to the sphere, and thus part of the errors in the new approximations is caused by the increasing complexity of the scattered fields as the scatterer boundary is approached. The Born and Rytov approximations (not shown) overshoot the amplitude by a factor of 3, as was seen in earlier examples for this conductivity ratio (10).

Figure 6 examines the residual norm for the model used in Figure 4 for conductivity ratios covering five orders of magnitude. We see that the new estimators provide exceptionally good estimates for a resistive inclusion, with the localized nonlinear (LN) approximation providing a slightly better estimate (1% error) than the SLNR (1.5% error) and SLN and LNR estimates (around 3% error). We have found that for resistive scatterers, the LN estimator is the best approximation, while its Rytov extension (LNR) is the worst. For a conducting inclusion the approximations provide good estimates for all three components up to contrast ratios around 20 where errors exceed 20%. Due to phase rotation of the scattered field, the LN is slightly better than the SLN, while the SLNR and LN are essentially equivalent. As the contrast ratio becomes higher, we found that the approximations significantly underestimate the magnitude and phase of the scattered H_y, and the norm thus approaches unity.

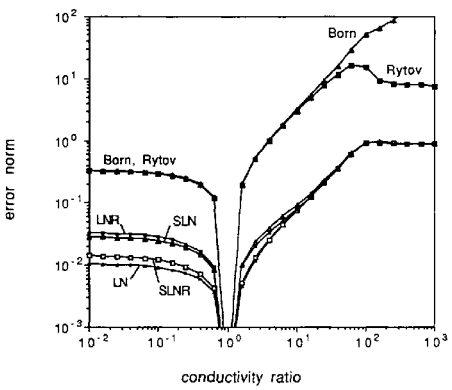

Fig. 6. The residual norm plotted as a function of conductivity ratio for a sphere of radius 30 m and a frequency of 100 Hz. The receiver and transmitter are as in Figure 4. Errors are less than 10% for conductivity ratios less than 10.

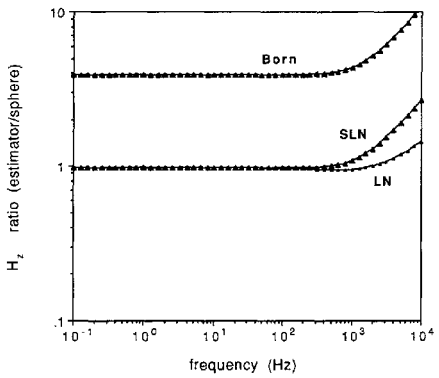

Fig. 7. The ratio of estimated to true amplitude of scattered H_z for the Born, SLN, and LN plotted as a function of frequency for the model of Figure 4. The new estimators are valid over a wide frequency range but become too large at high frequency. The LN provides a good estimate for this model well into the kilohertz range.

As frequency increases, the physics of the scattering changes as the effect of charges becomes less significant and induction becomes more significant. In Figures 7 and 8 we examine the accuracy of the approximations as a function of frequency. The conductivity ratio is fixed at 10, as in the previous example, and the sphere radius is 30 m. First, we examine just the SLN and LN approximations. Figure 7 compares the amplitude of the estimated solution to that of the true solution by plotting their ratio as function of frequency. The amplitude is given very accurately by both approximations for frequencies up to 300 Hz. Thereafter the LN approximation provides a better estimate of amplitude,

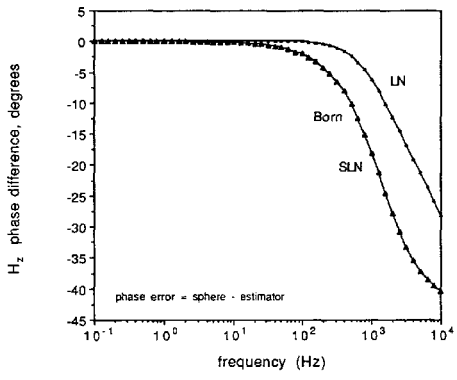

Fig. 8. The difference between the phase of the scattered H_z component for the true and the estimated solution as a function of frequency for the model in Figure 4. The LN estimator provides a phase improvement of up to 15° over the Born and SLN approximation, but the phase error becomes substantial at higher frequencies.

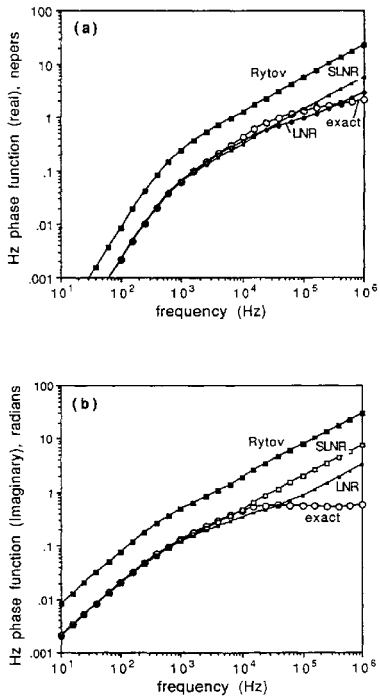

Fig. 9. The negative of the real and imaginary parts of the exact phase function (ψ), given by equation (41), and its estimates for the model of Figure 4. The new extended Rytov estimates (SLNR and LNR) are very accurate for frequencies up to 2000 Hz but eventually overestimate the magnitude of both the real and imaginary parts of the phase function. The magnitude of estimated total field is therefore too small and the phase too large.

until at 10 kHz it is in error by about 50%. In Figure 8, the phase error in the approximation of H_z is plotted as a function of frequency. The phase error is small for the Born and SLN estimators for frequencies up to 300 Hz but increases quickly thereafter as induction begins to contribute to the response. The scattered field for the static localized nonlinear (SLN) approximation does not correct the phase of the background field. The localized nonlinear (LN) approximation, on the other hand, provides a phase correction of up to 15° at high frequencies, resulting in a total phase error of 27° at 10 kHz. It correctly predicts the phase in this example up to 300 Hz.

In general, at low frequencies, the new approximations are quite accurate and considerably improve both amplitude and phase over the Born approximation. As the frequency increases, their accuracies differ, with the LN approximation providing both a better estimate of amplitude and phase than the SLN approximation. Eventually at high frequencies, the amplitude of the LN approximation becomes too large and the phase correction not sufficient, thus requiring the additional corrections anticipated by the Rytov extension.

At high frequencies, the true total field becomes small compared to the background field and thus the scattered field approaches the negative of the background. It is therefore appropriate, at such frequencies, to compare the accuracy of the approximations to the total field rather than scattered field as in the earlier figures. Since the background field decreases rapidly in amplitude as the frequency increases, we plot ratio of total field to background field. In this case, it is useful to compare the phase function estimates (equation (41)) of the various Rytov approximations to the logarithm of the exact ratio via equations (40) and (42).

In Figure 9, estimates of the total field for the previous model are plotted using the phase functions for the static localized nonlinear Rytov (SLNR), localized nonlinear Rytov (LNR), and the Rytov approximations up to frequencies of 1 MHz. The negatives of both the real and imaginary parts of the phase functions are plotted in Figure 9. The real part of the phase function is the logarithm of the amplitude of the ratio of the total field to the background field. The exact total field becomes small compared to the background field as the frequency increases. The Rytov approximation overestimates this decay, so that the Rytov estimate of the total field quickly vanishes with respect to the background field. The LNR and SLNR provide accurate estimates of the total field amplitude for frequencies up to several kilohertz. For two decades higher, they slightly underestimate the decay rate, and then beyond 100 kHz they overestimate the total field which decays to zero. The imaginary part of the phase function is the phase of the total field compared to the background. The Rytov approximation overestimates this phase rotation at all frequencies, while the two new Rytov approximations (SLNR and LNR) provide accurate estimates for frequencies up to several kilohertz. Thereafter, the SLNR provides the best estimate of the phase rotation until the imaginary part of the exact phase function asymptotes after 10 kHz.

The phase error of the estimates is also a function of the conductivity ratio. In Figure 10, we look more closely at the phase of the scattered H_z field component for both resistive

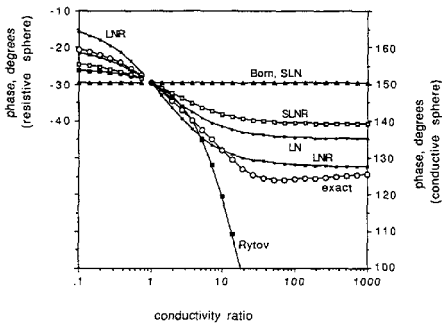

Fig. 10. Phase of the scattered H_z component as a function of conductivity ratio at 1000 Hz (note the 180° phase change between resistive and conductive inclusions). The LNR approximation estimates the phase to within a few degrees for positive conductivity contrasts and provides a further improvement in phase from the LN. For resistive inclusions, the LN estimator is most accurate.

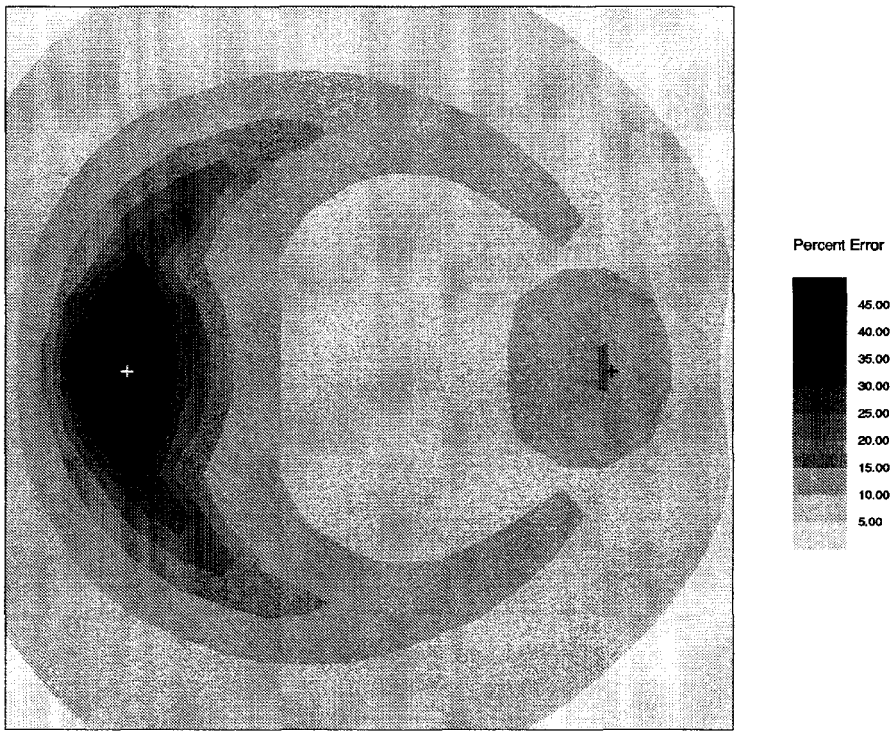

Fig. 11. Plan view (in the x-y plane) of the contoured error residual for the scattered magnetic field expressed as a percent error for the localized nonlinear estimator when the sphere is centered in the $z = 35$ m plane. The sphere has a radius of 30 m and conductivity of 1 S/m, the background conductivity is 0.1 S/m, and the frequency is 100 Hz. The Tx is below the white cross, while the receivers are below the black cross. Both Tx and Rx are in the $z = 0$ plane with the Tx moment perpendicular to the contour plane. Errors are generally less than 20% but are highest in the vicinity of the transmitter.

and conductive inclusions at an excitation frequency of 1 kHz within the range of accuracy of the Rytov extensions, SLNR and LNR as demonstrated in Figure 9. The LN approximation provides extremely accurate phase estimates for resistive scatterers (conductivity ratios less than 1), while the phase of the SLN approximation becomes significantly in error for large ratios. The Rytov and the SLNR approximations underestimate the phase anomaly by about 5°, while the LNR approximation overestimates the phase anomaly by about 5°. The phase anomaly is relatively small for resistive inclusions, and the misfit is never large. The LN approximation provides the best estimates. For conducting spheres, however, the phase anomaly can become substantial. As the sphere becomes more conducting the phase of the scattered field deviates from that of the background by more than 25° for conductivity ratios larger than 30. The localized nonlinear approximation tracks this phase anomaly initially but underestimates the large-ratio asymptote by around 10°. The SLNR provides a better estimate than the SLN estimate, while the LNR approximation tracks the phase anomaly best for large ratios of conductivity, being in error by less than 5°.

The accuracy of the approximations is not only a function of conductivity ratio, frequency, and size of the scatterer but is also a function of the geometry of the exciting field and the location of the receiver. In Figure 11 we plot the residual norm for the localized nonlinear approximation as the origin of a 30-m-radius sphere is varied for fixed transmitter and receiver locations, conductivity, and frequency. The center of the spherical scatterer is moved within the plane $Z = 35$ m. The transmitter is located below the white cross at $Z = 0$ and is oriented normal to the plane. Thus the spherical scatterers come within 5 m of the Tx-Rx plane. The receiver location is 200 m away from the transmitter, below the black cross. The frequency of excitation is 100 Hz so that the LN approximation is sufficient. The LN approximation is very good over most of the region except when the sphere is

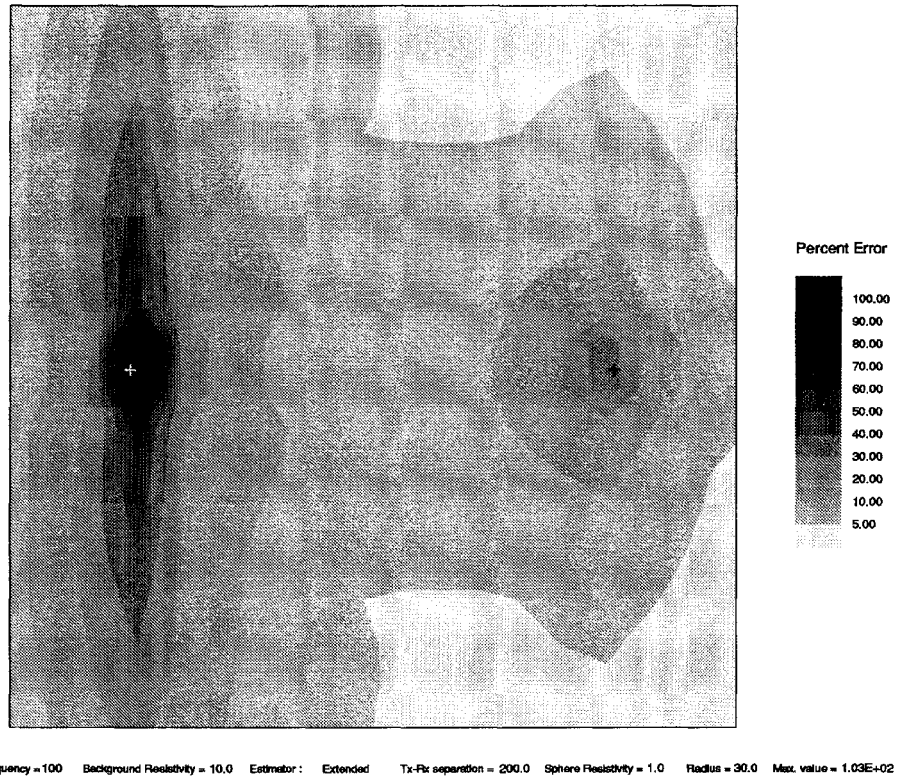

Fig. 12. Section view (in the y-z plane) of the contoured error residual for the scattered magnetic field expressed as a percent error for localized nonlinear estimator when the sphere is centered in the $x = 35$ m plane. The model is the same as in Figure 11. The Tx is behind the white cross while the receivers are behind the black cross. Both Tx and Rx are in the $x = 0$ plane. The error is highest along the axis of the transmitter.

located above the transmitter, where a maximum error of 45% is obtained. Figure 12 shows a section view of the same model, with the plane of the sphere centers at $X = 35$ m. Again, the estimator is very good except when the source is near the scatterer and is poorest when the scatterer is near the axis of the source. The misfit of the approximations is associated, at least partly, with the geometry of the scatterer. This is directly related to the geometry of the total internal electric field which we examine more closely in Appendix C. Also, in Appendix C, we include an example of the external scattered electric field estimates from the new approximations.

Discussion and Conclusions

In electromagnetic scattering from a conductive inclusion, the Born and Rytov approximations give accurate estimates of the scattered field only when the contrasts in physical property and scatterer size are small. For example, at 100 Hz the Born approximation is accurate to within 20% for a 1-m sphere located 10 m from both the source and receiver for conductivity contrasts of 1:1.5. The error rises rapidly to 400% at a conductivity contrast of 1:10. The static localized nonlinear (SLN) approximation provides a significantly improved estimate of the amplitudes of the scattered fields for a wide range of conductivity contrasts, scatterer size and exciting frequency (for the 1-m sphere, the error is only 0.5% for a contrast of 1:10). However, as with the traditional Born approximation, the SLN approximation does not provide a good estimate of the phase of the scattered field. The localized nonlinear approximation provides some phase correction and an additional amplitude correction to extend the range of application. These corrections have reduced accuracy for particular source-scatterer geometries, especially on the axis of the dipolar source, and are less applicable at high frequencies with large scatterers. The localized nonlinear Rytov approximation provides mainly additional phase cor-

rections and some amplitude correction to the simpler localized nonlinear approximation at higher frequencies for larger scatterers and higher positive conductivity contrasts. In some cases, particularly at high frequencies, the static localized nonlinear Rytov approximation is superior to the full localized nonlinear Rytov approximation which is contrary to what one would expect. Detailed studies, such as those described here, should be done to select the most appropriate approximation for specific applications.

To use these approximations for forward modeling, it is first necessary to derive the depolarization tensor for elementary scatterers more suitable as building blocks for complex geometries than spheres. The formulation outlined in this paper is presently being generalized to geometries such as rectangular parallelepiped and rectangular cylinders. Investigation of the use of the approximation in multiple scattering interactions must also be done prior to building a forward modeling tool.

The new approximations also open the possibility of fast nonlinear inversion. These new approximations can also be generalized to more complex background media, where they can significantly improve the performance of iterative inversion algorithms based on the distorted-wave Born and Rytov approximations.

Appendix A: Derivation of the Localized Nonlinear Approximation of the Internal Electric Field for a Spherical Scatterer

The new approximations depend on the geometry of the scatterer. In this appendix we derive detailed expressions for the internal electric field inside a homogeneous spherical scatterer in a uniform whole space. The technique used here is specific to a spherical geometry.

For $\mathbf{r} \in V_s$ the internal electric field is approximated by equation (31):

$$\mathbf{E}(\mathbf{r}) \approx \bar{\bar{\Gamma}}(\mathbf{r}) \cdot \mathbf{E}_b(\mathbf{r}), \tag{A1}$$

where from equation (30),

$$\bar{\bar{\Gamma}}(\mathbf{r}) = \left[\bar{\bar{I}} + \frac{\Delta\sigma}{\sigma_b}\bar{\bar{L}}(\mathbf{r})\right]^{-1} \tag{A2}$$

$$\bar{\bar{L}}(\mathbf{r}) = -[k_b^2\bar{\bar{I}} + \nabla\nabla]f(\mathbf{r}), \tag{A3}$$

$$f(\mathbf{r}) = \int_{V_s} d\mathbf{r}'\, g(\mathbf{r}, \mathbf{r}'). \tag{A4}$$

To obtain the depolarization tensor, we begin by expanding the scalar Green's function in terms of spherical Bessel functions and Hankel functions of the first kind [*Morse and Feshbach*, 1953]

$$g(\mathbf{r}, \mathbf{r}') = \frac{ik_b}{4\pi}\sum_{n=0}^{\infty}(2n+1) \cdot \sum_{m=0}^{n}\chi_m\frac{(n-m)!}{(n+m)!}P_n^m(\cos\theta)P_n^m(\cos\theta') \cdot \cos[m(\phi-\phi')]\begin{cases} j_n(k_br')h_n^{(1)}(k_br), & r \geq r' \\ j_n(k_br)h_n^{(1)}(k_br'), & r \leq r' \end{cases} \tag{A5}$$

where

$$\chi_m = \begin{cases} 1, & m = 0 \\ 2 & m \neq 0. \end{cases}$$

Setting the origin at the center of the sphere

$$f(\mathbf{r}) = ik_b\left[h_0^{(1)}(k_br)\int_0^r dr'\, r'^2 j_0(k_br') + j_0(k_br)\int_r^a dr'\, r'^2 h_0^{(1)}(k_br')\right] = \frac{1}{k_b^2}\left[-1 + \psi(k_ba)\frac{\sin(k_br)}{k_br}\right] \tag{A6}$$

where the zero-order spherical functions are given by

$$h_0^{(1)}(z) = -i\frac{e^{iz}}{z}, \qquad j_0(z) = \sin z/z \tag{A7}$$

and

$$\psi(k_ba) = (1 - ik_ba)e^{ik_ba}. \tag{A8}$$

Due to the spherical symmetry of the sphere

$$\nabla f(\mathbf{r}) = f'(\mathbf{r})\hat{\mathbf{r}} \tag{A9}$$

where $f'(\mathbf{r})$ is the derivative of $f(\mathbf{r})$ with respect to r. Thus

$$-\bar{\bar{L}}(\mathbf{r}) = k_b^2 f(\mathbf{r})\bar{\bar{I}} + \nabla\nabla f(\mathbf{r}) = k_b^2 f(\mathbf{r})\bar{\bar{I}} + \left[f''(\mathbf{r}) - \frac{f'(\mathbf{r})}{r}\right]\hat{\mathbf{r}}\hat{\mathbf{r}} + \frac{f'(\mathbf{r})}{r}\bar{\bar{I}} = h(\mathbf{r})\bar{\bar{I}} + p(\mathbf{r})\hat{\mathbf{r}}\hat{\mathbf{r}}. \tag{A10}$$

Evaluating the derivatives of $f(\mathbf{r})$ in equation (A10), we have

$$h(\mathbf{r}) = k_b^2 f(\mathbf{r}) + \frac{f'(\mathbf{r})}{r} = -1 + \frac{\psi(k_ba)}{k_br} \cdot \left[\sin(k_br) + \frac{\cos(k_br)}{k_br} - \frac{\sin(k_br)}{(k_br)^2}\right], \tag{A11a}$$

$$p(\mathbf{r}) = f''(\mathbf{r}) - \frac{f'(\mathbf{r})}{r} = -\frac{\psi(k_ba)}{k_br} \cdot \left[\sin(k_br) + 3\frac{\cos(k_br)}{k_br} - 3\frac{\sin(k_br)}{(k_br)^2}\right]. \tag{A11b}$$

The low-frequency asymptotes, when $|k_ba| \ll 1$, are given by

$$h(\mathbf{r}) \approx -\tfrac{1}{3} + \tfrac{1}{3}(k_ba)^2 - \tfrac{2}{15}(k_br)^2, \tag{A12a}$$

$$p(\mathbf{r}) \approx \tfrac{1}{15}(k_br)^2. \tag{A12b}$$

In the DC limit,

$$h(\mathbf{r}) \to -\tfrac{1}{3}, \tag{A13a}$$

$$p(\mathbf{r}) \to 0, \tag{A13b}$$

and therefore from equation (A10),

$$\bar{\bar{L}}(\mathbf{r}) = \tfrac{1}{3}\,\bar{\bar{I}}, \tag{A14}$$

and

$$\bar{\bar{\Gamma}}_0(\mathbf{r}) = \left(1 + \frac{1}{3}\frac{\Delta\sigma}{\sigma_b}\right)^{-1}\bar{\bar{I}} = \left(\frac{3\sigma_b}{\sigma + 2\sigma_b}\right)\bar{\bar{I}}. \tag{A15}$$

Thus, from (A1), the internal electric field under the SLN approximation is given by

$$\mathbf{E}(\mathbf{r}) \approx \left(\frac{3\sigma_b}{\sigma + 2\sigma_b}\right)\mathbf{E}_b(\mathbf{r}), \qquad \mathbf{r} \in V_s. \tag{A16}$$

To obtain a closed form expression for the internal field for all frequencies, we invert (A1) for the spherical scatterer

$$\begin{aligned}\mathbf{E}_b(\mathbf{r}) = \bar{\bar{\Gamma}}^{-1}(\mathbf{r}) \cdot \mathbf{E}(\mathbf{r}) &= \left[\bar{\bar{I}} - \frac{\Delta\sigma}{\sigma_b}\,\bar{\bar{L}}(\mathbf{r})\right] \cdot \mathbf{E}(\mathbf{r}) \\ &= \left(1 - \frac{\Delta\sigma}{\sigma_b}\,h(\mathbf{r})\right)\mathbf{E}(\mathbf{r}) - \frac{\Delta\sigma}{\sigma_b}\,p(\mathbf{r})\hat{\mathbf{r}}\hat{\mathbf{r}} \cdot \mathbf{E}(\mathbf{r})\end{aligned} \tag{A17}$$

and therefore

$$\begin{aligned}\hat{\mathbf{r}} \cdot \mathbf{E}_b(\mathbf{r}) &= \left(1 - \frac{\Delta\sigma}{\sigma_b}\,h(\mathbf{r})\right)\hat{\mathbf{r}} \cdot \mathbf{E}(\mathbf{r}) - \frac{\Delta\sigma}{\sigma_b}\,p(\mathbf{r})\hat{\mathbf{r}} \cdot \mathbf{E}(\mathbf{r}) \\ &= \left(1 - \frac{\Delta\sigma}{\sigma_b}\,s(\mathbf{r})\right)\hat{\mathbf{r}} \cdot \mathbf{E}(\mathbf{r}),\end{aligned} \tag{A18}$$

where

$$s(\mathbf{r}) = h(\mathbf{r}) + p(\mathbf{r}). \tag{A19}$$

Substituting $\hat{\mathbf{r}} \cdot \mathbf{E}(\mathbf{r})$ from equation (A18) in equation (A17)

$$\mathbf{E}_b(\mathbf{r}) = \left(1 - \frac{\Delta\sigma}{\sigma_b}\,h(\mathbf{r})\right)\mathbf{E}(\mathbf{r}) - \frac{\Delta\sigma}{\sigma_b}\,p(\mathbf{r})\,\frac{\hat{\mathbf{r}} \cdot \mathbf{E}_b(\mathbf{r})}{[1 - (\Delta\sigma/\sigma_b)s(\mathbf{r})]}\,\hat{\mathbf{r}}, \tag{A20}$$

and thus the internal electric field can be expressed explicitly in terms of the background field and functions which are dependent on geometry, frequency, and the conductivity of the background medium,

$$\mathbf{E}(\mathbf{r}) = \left(1 - \frac{\Delta\sigma}{\sigma_b}\,h(\mathbf{r})\right)^{-1}\left[\mathbf{E}_b(\mathbf{r}) + \frac{\Delta\sigma}{\sigma_b}\,p(\mathbf{r})\,\frac{\hat{\mathbf{r}} \cdot \mathbf{E}_b(\mathbf{r})}{1 - (\Delta\sigma/\sigma_b)s(\mathbf{r})}\,\hat{\mathbf{r}}\right], \qquad \mathbf{r} \in V_s. \tag{A21}$$

For most geophysical applications, the secondary or total fields outside the scatterer are the chief interest. The precise formulations used for calculating the fields outside the scatterer are derived in Appendix B.

Appendix B: Derivation of the External Scattered Fields for a Spherical Scatterer Under the Localized Nonlinear Approximation

In this appendix we derive explicit expressions for the external magnetic and electric scattered fields under the localized nonlinear approximation for a spherical scatterer. The expressions are suitable for rapid numerical calculation.

Magnetic Field

From equation (35), the scattered magnetic field is given by

$$\mathbf{H}_s(\mathbf{r}) = \Delta\sigma \int_{V_s} d\mathbf{r}'\,[\nabla g(\mathbf{r}, \mathbf{r}')] \times \mathbf{E}(\mathbf{r}'). \tag{B1}$$

Its component along $\hat{\mathbf{u}}$ is given by

$$\begin{aligned}H_s^u(\mathbf{r}) &= \Delta\sigma \int_{V_s} d\mathbf{r}'\,\{-\nabla g(\mathbf{r}, \mathbf{r}') \cdot [\hat{\mathbf{u}} \times \mathbf{E}(\mathbf{r}')]\} \\ &= \Delta\sigma \int_{V_s} d\mathbf{r}'\,F_u(\mathbf{r}, \mathbf{r}'), \qquad \mathbf{r} \notin V_s\end{aligned} \tag{B2}$$

where, from equation (48) for the internal electric field, we have

$$\hat{\mathbf{u}} \times \mathbf{E}(\mathbf{r}') \approx \left(1 - \frac{\Delta\sigma}{\sigma_b}\,h(\mathbf{r}')\right)^{-1}\left[\hat{\mathbf{u}} \times \mathbf{E}_b(\mathbf{r}') + \frac{\Delta\sigma}{\sigma_b}\,p(\mathbf{r}')\,\frac{\hat{\mathbf{r}} \cdot \mathbf{E}_b(\mathbf{r}')}{1 - (\Delta\sigma/\sigma_b)s(\mathbf{r}')}\,\hat{\mathbf{u}} \times \hat{\mathbf{r}}'\right]. \tag{B3}$$

We consider an infinitesimal magnetic dipole source oriented along $\hat{\mathbf{z}}$ and located at $\mathbf{r}_s$. The background electric field is given by

$$\mathbf{E}_b(\mathbf{r}') = m\hat{\mathbf{z}} \times \nabla' g(\mathbf{r}', \mathbf{r}_s) \tag{B4}$$

where m is the source moment. Since

$$\hat{\mathbf{u}} \times \{\hat{\mathbf{z}} \times \nabla' g(\mathbf{r}', \mathbf{r}_s)\} = \hat{\mathbf{z}}\{\hat{\mathbf{u}} \cdot \nabla' g(\mathbf{r}', \mathbf{r}_s)\} - (\hat{\mathbf{z}} \cdot \hat{\mathbf{u}})\nabla' g(\mathbf{r}', \mathbf{r}_s) \tag{B5}$$

and

$$\begin{aligned}\hat{\mathbf{r}}' \cdot \mathbf{E}_b(\mathbf{r}') &= m\hat{\mathbf{r}}' \cdot \{\hat{\mathbf{z}} \times \nabla' g(\mathbf{r}', \mathbf{r}_s)\} \\ &= m(\hat{\mathbf{r}}' \times \hat{\mathbf{z}}) \cdot \nabla' g(\mathbf{r}', \mathbf{r}_s)\end{aligned} \tag{B6}$$

then

$$\begin{aligned}F_u(\mathbf{r}, \mathbf{r}') = m\left(1 - \frac{\Delta\sigma}{\sigma_b}\,h(\mathbf{r}')\right)^{-1} &\cdot \Big\{(\hat{\mathbf{z}} \cdot \hat{\mathbf{u}})\{\nabla g(\mathbf{r}, \mathbf{r}')\} \cdot [\nabla' g(\mathbf{r}', \mathbf{r}_s)] \\ &- [\hat{\mathbf{z}} \cdot \nabla g(\mathbf{r}, \mathbf{r}')][\hat{\mathbf{u}} \cdot \nabla' g(\mathbf{r}', \mathbf{r}_s)] \\ &+ \frac{\Delta\sigma}{\sigma_b}\,p(\mathbf{r}')\left(1 - \frac{\Delta\sigma}{\sigma_b}\,s(\mathbf{r}')\right)^{-1}[(\hat{\mathbf{z}} \times \hat{\mathbf{r}}')\end{aligned}$$

$$\cdot \nabla' g(\mathbf{r}', \mathbf{r}_s)][(\hat{\mathbf{u}} \times \hat{\mathbf{r}}') \cdot \nabla g(\mathbf{r}, \mathbf{r}')]\Big\}$$

$$= mB_0(r')\{(\hat{\mathbf{z}} \cdot \hat{\mathbf{u}})[\nabla g(\mathbf{r}, \mathbf{r}')]$$

$$\cdot [\nabla' g(\mathbf{r}', \mathbf{r}_s)] - [\hat{\mathbf{z}} \cdot \nabla g(\mathbf{r}, \mathbf{r}')][\hat{\mathbf{u}} \cdot \nabla' g(\mathbf{r}', \mathbf{r}_s)]$$

$$+ B_1(r')[(\hat{\mathbf{z}} \times \hat{\mathbf{r}}') \cdot \nabla' g(\mathbf{r}', \mathbf{r}_s)][(\hat{\mathbf{u}} \times \hat{\mathbf{r}}') \cdot \nabla g(\mathbf{r}, \mathbf{r}')]\}. \tag{B7}$$

For the Born approximation

$$B_0(r') = 1, \qquad B_1(r') = 0 \tag{B8}$$

while for the static localized nonlinear (SLN) approximation

$$B_0(r') = \left(1 + \frac{\Delta\sigma}{3\sigma_b}\right)^{-1}, \qquad B_1(r') = 0 \tag{B9}$$

and for the localized nonlinear (LN) approximation

$$B_0(r') = \left(1 - \frac{\Delta\sigma}{\sigma_b} h(\mathbf{r}')\right)^{-1},$$

$$B_1(r') = \frac{\Delta\sigma}{\sigma_b} p(\mathbf{r}')\left(1 - \frac{\Delta\sigma}{\sigma_b} s(\mathbf{r}')\right)^{-1} \tag{B10}$$

where $h(\mathbf{r}')$, $p(\mathbf{r}')$, and $s(\mathbf{r}')$ are calculated from equation (50).

As an example, consider $\hat{\mathbf{u}} = \hat{\mathbf{z}}$, the origin at $\mathbf{r}_0$, the transmitter at $\mathbf{r}_s$, the receiver at $\mathbf{r}$, and the probed point within the scatterer at $\mathbf{r}'$. Then

$$F_z(\mathbf{r}, \mathbf{r}_s; \mathbf{r}') = mB_0(|\mathbf{r}' - \mathbf{r}_0|)\Big\{\frac{\partial g(\mathbf{r}, \mathbf{r}')}{\partial x}\frac{\partial g(\mathbf{r}', \mathbf{r}_s)}{\partial x'}$$

$$+ \frac{\partial g(\mathbf{r}, \mathbf{r}')}{\partial y}\frac{\partial g(\mathbf{r}', \mathbf{r}_s)}{\partial y'} + \frac{B_1(|\mathbf{r}' - \mathbf{r}_0|)}{|\mathbf{r}' - \mathbf{r}_0|^2}$$

$$\cdot \left[(x' - x_0)\frac{\partial g(\mathbf{r}', \mathbf{r}_s)}{\partial y'} - (y' - y_0)\frac{\partial g(\mathbf{r}', \mathbf{r}_s)}{\partial x'}\right]$$

$$\cdot \left[(x' - x_0)\frac{\partial g(\mathbf{r}, \mathbf{r}')}{\partial y} - (y' - y_0)\right.$$

$$\left.\cdot \frac{\partial g(\mathbf{r}, \mathbf{r}')}{\partial x}\right]\Big\} = -\frac{m}{(4\pi)^2} B_0(|\mathbf{r}' - \mathbf{r}_0|)$$

$$\cdot \frac{e^{ik_b|\mathbf{r}' - \mathbf{r}|}}{|\mathbf{r}' - \mathbf{r}|^3}\frac{e^{ik_b|\mathbf{r}' - \mathbf{r}_s|}}{|\mathbf{r}' - \mathbf{r}_s|^3}$$

$$\cdot [1 - ik_b|\mathbf{r}' - \mathbf{r}|][1 - ik_b|\mathbf{r}' - \mathbf{r}_s|]$$

$$\cdot \Big[(x' - x)(x' - x_s) + (y' - y)(y' - y_s)$$

$$+ \frac{B_1(|\mathbf{r}' - \mathbf{r}_0|)}{|\mathbf{r}' - \mathbf{r}_0|^2} \cdot [(x' - x_0)(y' - y)$$

$$- (y' - y_0)(x' - x)][(x' - x_0)$$

$$\cdot (y' - y_s) - (y' - y_0)(x' - x_s)]\Big\}. \tag{B11}$$

Electric Field

The estimated total or scattered electric field outside the sphere are computed by numerically evaluating the volume integral of equation (7) with the internal electric field approximated by equation (48). The scattered electric field is given by

$$\mathbf{E}_s(\mathbf{r}) = i\omega\mu_0\Delta\sigma \int_{V_s} d\mathbf{r}' \, \bar{\bar{G}}(\mathbf{r}, \mathbf{r}') \cdot \mathbf{E}(\mathbf{r}'), \tag{B12}$$

where the dyadic Green's function is given by equation (5). The contribution to the ith element of the vector integrand of (B12) from the derivative portion of the dyadic Green's function is

$$\{\nabla\nabla \cdot [g(\mathbf{r}, \mathbf{r}')\mathbf{E}(\mathbf{r}')]\}_i = \sum_{j=1}^{3} K_{ij}(\mathbf{r}, \mathbf{r}')E_j(\mathbf{r}'), \tag{B13}$$

where

$$K_{ij}(\mathbf{r}, \mathbf{r}') = \frac{\partial^2 g(\mathbf{r}, \mathbf{r}')}{\partial x_i \partial x_j}$$

$$= -\frac{g(\mathbf{r}, \mathbf{r}')}{|\mathbf{r} - \mathbf{r}'|^2}\Big\{[1 - ik_b|\mathbf{r} - \mathbf{r}'|]\delta_{ij}$$

$$- \frac{(x_i - x_i')}{|\mathbf{r} - \mathbf{r}'|}\frac{(x_j - x_j')}{|\mathbf{r} - \mathbf{r}'|}$$

$$\cdot [3 - 3ik_b|\mathbf{r} - \mathbf{r}'| - k_b^2|\mathbf{r} - \mathbf{r}'|^2]\Big\}. \tag{B14}$$

The elements of the dyadic Green's function are simply

$$G_{ij}(\mathbf{r}, \mathbf{r}') = g(\mathbf{r}, \mathbf{r}')\delta_{ij} + \frac{1}{k_b^2} K_{ij}(\mathbf{r}, \mathbf{r}'). \tag{B15}$$

To determine the ith component of the external electric field at a field point $\mathbf{r}$, a numerical integration over the volume of the scatterer is performed, giving

$$E_{si}(\mathbf{r}) \approx i\omega\mu_0\Delta\sigma \int_{V_s} d\mathbf{r}' \sum_{j=1}^{3} G_{ij}(\mathbf{r}, \mathbf{r}')\hat{E}_j(\mathbf{r}') \tag{B16}$$

where the estimated internal electric field $\hat{E}_j(\mathbf{r}')$ is calculated either from equation (48) under the LN approximation or from equation (55) under the SLN approximation.

Appendix C: Electric Fields of a Spherical Scatterer—Numerical Results

Internal Electric Field

To better understand the approximations of the fields, we examine in detail the field that is crucial to all the approximations: the total internal electric field. We begin with a

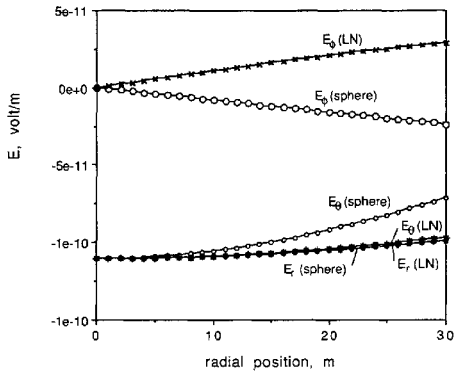

Fig. C1. The internal electric field as a function of radial position from the sphere center: $Tx = (r, \theta, \phi) = (100, 90°, -45°)$ and $Rx = (\theta, \phi) = (45°, 45°)$. The sphere center is at (0,0,0).

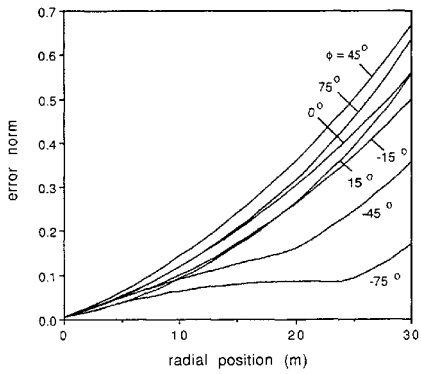

Fig. C2. The residual norm for the internal electric field as a function of radial position and azimuthal angle for a fixed theta angle ($\theta = 30°$).

model for which the approximations give moderate accuracy. The radius of the sphere is fairly large (30 m), the frequency is moderate (100 Hz), the conductivity contrast is 10:1 (σ: σ_B = 1:0.1 S/m). The sphere is located at the origin, the Tx is located at $\phi = 45°$ and at a distance of 100 m away from the sphere center. The transmitter is pointing along the z axis.

Figure C1 compares the in-phase electric field as a function of radial distance from the sphere center along a profile with a fixed θ and ϕ. The true solution for the total field, represented in spherical components, is compared to that of the localized nonlinear (LN) approximation. The radial component ($e_r\hat{r}$) closely matches the true solution for all radial locations, while the θ component ($e_\theta\hat{\theta}$) matches near the sphere center but diverges from the true solution as the surface of the sphere is approached. The ϕ component ($e_\phi\hat{\phi}$), although small, has the wrong sign (i.e., wrong direction).

For $\theta = 30°$, Figure C2 examines the residual norm for the total internal field as a function of both radius and azimuthal angle. The residual error is small at the center but increases toward the surface of the sphere. The approximations are more accurate for positions on the near side of sphere relative to the Tx ($\phi = [-15°, -75°]$) than on the far side ($\phi = [0°, 75°]$).

In general, the approximations do not determine accurately those components of the internal electrical field which become tangential to the surface of the sphere as the surface of the sphere is approached, i.e., the θ and ϕ components. On the other hand, the radial component, which is normal to the sphere surface, is always determined relatively accurately.

The preceding results give some insight into the comparisons made earlier on the external electromagnetic field components. The external scattered magnetic field is determined by a volume integration of the total internal field over V_s. Our studies have shown that the main contribution to this volume integration is mainly from internal points which are close to the surface of the sphere. In addition, the gradients in the θ and ϕ components increase with the size of the sphere. The poor approximation of the θ and ϕ components of the internal field away from the sphere center combined with the large gradients of these components for larger spheres, is responsible for the misfit of the external scattered magnetic fields.

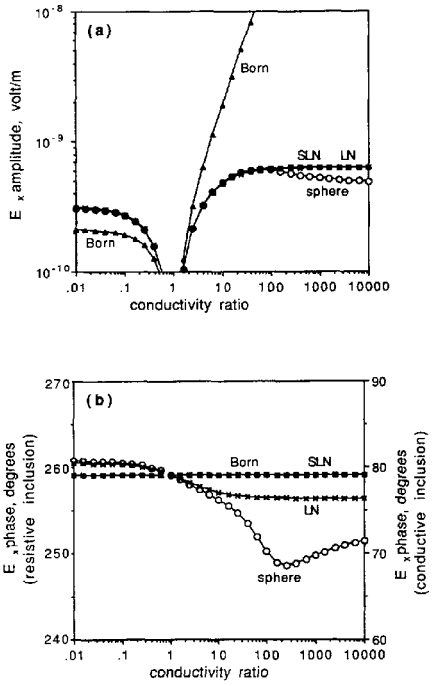

Fig. C3. The scattered electric fields external to the sphere. The model and Tx and Rx locations are the same as in Figure 4.

The orientation and location of the transmitter determine the relative importance of the tangential and normal components in the determination of the external scattered fields. For example, when the dipole axis of the source intersects the scatterer, the tangential components are relatively larger than when the center of the scatterer is on an axis perpendicular to the axis of the source. For a resistive inclusion, the internal field is only slightly larger than the background field. However, for a conductive inclusion the internal field is often significantly smaller than the external field. Thus, for the resistive inclusion the variation of the tangential components from the center to outside the scatterer is less than for the conducting case. As the frequency increases or the sphere becomes larger, gradients in the θ and ϕ components increase due to inductive loss and phase rotation effects, thereby increasing the inaccuracy of the internal estimates.

External Electric Field

For locations external to the sphere the scattered electric field $\mathbf{E}_s$ is calculated by volume integration over the support of Q by the use of equations (B16) and (48).

As an example, we calculate $\mathbf{E}_s$ for the Rx position and the model used in Figure 4. At this Rx location, there is only one component of the scattered field, E_x. In Figure C3 we plot the true solution and the three approximations, Born, LN, and SLN. The LN and SLN approximations to the amplitude are good to within 1.5% for conductivity ratios up to about 100, beyond which the estimated amplitude diverges from its true value. The LN estimator tracks the phase reasonably well to within 2° up to conductivity ratios of about 25 but fails to estimate the true phase for more conductive spheres.

Acknowledgments. We would like to thank Michael Oristaglio and Carlos Torres-Verdin for invaluable discussions and suggestions on improving the manuscript. We would also like to thank David Johnson, Apo Sezginer, Douglas Oldenburg, Ari Ben-Menahem, Ki Ha Lee, and Gregory Newman for their invaluable feedback.

REFERENCES

Born, M., *Optik*, Springer-Verlag, New York, 1933.
Born, M., and E. Wolf, *Principles of Optics*, 808 pp., Pergamon, New York, 1980.
Habashy, T. M., W. C. Chew, and E. Y. Chow, Simultaneous reconstruction of permittivity and conductivity profiles in a radially inhomogeneous slab, *Radio Sci.*, *21*(4), 635–645, 1986.
Habashy, T. M., E. Y. Chow, and D. G. Dudley, Profile inversion using the renormalized source-type integral equation approach, *IEEE Trans. Antennas Propag.*, *AP-38*(5), 668–682, 1990.
Jackson, J. D., *Classical Electrodynamics*, 848 pp., John Wiley, New York, 1975.
Kak, A. C., and M. Slaney, *Principles of Computerized Tomographic Imaging*, 329 pp., IEEE Press, New York, 1988.
Keller, J. B., Accuracy and validity of the Born and Rytov approximations, *J. Opt. Soc. Am.*, *59*, 1003–1004, 1969.
Kong, J. A., *Electromagnetic Wave Theory*, 696 pp., Wiley-Interscience, New York, 1986.
Lindell, I. V., TE/TM decomposition of electromagnetic sources, *IEEE Trans. Antennas Propag.*, *AP-36*(10), 1382–1388, 1988.
Morse, P. M., and H. Feshbach, *Methods of Theoretical Physics*, Part II, 1978 pp., McGraw-Hill, New York, 1953.
Newton, R. G., *Scattering Theory of Waves and Particles*, 681 pp., McGraw-Hill, New York, 1966.
Nieto-Vesperinas, M., *Scattering and Diffraction in Physical Optics*, 397 pp., John Wiley, New York, 1991.
Oristaglio, M. L., Accuracy of the Born and Rytov approximations for reflection and refraction at a plane interface, *J. Opt. Soc. Am. A*, *2*, 1987–1993, 1985.
Oristaglio, M. L., An inverse scattering formula that uses all the data, *Inverse Problems*, *5*, 1097–1105, 1989.
Sancer, M. I., and A. D. Varvatsis, A comparison of the Born and Rytov methods, *Proc. IEEE*, *58*, 140–141, 1970.
Sobczyk, K., *Stochastic Wave Propagation*, 248 pp., Elsevier, New York, 1985.
Tatarskii, V. I., *The Effects of the Turbulent Atmosphere on Wave Propagation*, 472 pp., translated from Russian, National Oceanic and Atmospheric Administration, U.S. Department of Commerce and the National Science Foundation, Washington, D. C., 1971.
Van Kranendonk, J., and J. E. Sipe, Foundations of the macroscopic electromagnetic theory of dielectric medium, *Prog. Opt.*, *15*, 245–350, 1977.
Yaghjian, A. D., Electric dyadic Green's functions in the source region, *Proc. IEEE*, *68*, 248–263, 1980.

R. W. Groom, T. M. Habashy, and B. R. Spies, Schlumberger-Doll Research, Old Quarry Road, Ridgefield, CT 06877-4108.

(Received April 1, 1992;
revised September 10, 1992;
accepted October 2, 1992.)